

## Measurements of the Polarization in Proton-Proton Elastic Scattering from 2.50 to 5.15 GeV/c<sup>\*†</sup>

J. H. Parry,<sup>‡</sup> N. E. Booth,<sup>§</sup> G. Conforto,<sup>||</sup> R. J. Esterling,<sup>||</sup> J. Scheid,<sup>§</sup> and D. J. Sherden<sup>\*\*</sup>

*University of Chicago and Enrico Fermi Institute, Chicago, Illinois 60637*

A. Yokosawa

*Argonne National Laboratory, Argonne, Illinois 60439*

(Received 10 August 1972)

In an experiment at the Argonne Zero-Gradient Synchrotron we have measured values of the polarization parameter  $P(t)$  in the elastic scattering of negative pions, positive pions, positive kaons, and protons on protons at several incident laboratory momenta from 2.50 to 5.15 GeV/c, and for values of the momentum transfer variable  $-t$  from 0.2 to 2.0 (GeV/c)<sup>2</sup>. The final results from  $p$ - $p$  elastic scattering presented here extend our knowledge of the polarization to much larger values of  $-t$  than the results of previous measurements. Outstanding features revealed by these polarization data include (1) the development of a dip at about  $-t = 0.7$  (GeV/c)<sup>2</sup>, with (2) a substantial secondary peak at larger values of  $-t$  and (3) the gradual diminution of the maximum polarization with increasing energy. It is possible to fit the  $t$  dependence of the experimental results with a simple model. The energy dependence of the polarized cross sections is also discussed.

### I. INTRODUCTION

The study of the proton-proton interaction continues to be one of the central problems of high-energy physics. The high-energy behavior of the total cross section and the energy and angular dependence of the differential cross section continue to receive a great deal of attention, both theoretical and experimental. One of the goals of these studies is to achieve a realistic picture of the interaction of hadrons at high energies, in spite of the fact that we might expect the proton-proton interaction to be extremely complicated. The use of partial-wave expansions at high energies involves, with the present experimental data, far too many unknown partial-wave amplitudes. To describe the scattering in terms of helicity amplitudes requires five complex amplitudes which (without a model) are independent. The Regge-pole model has been able to explain some of the general features of the experiments, but it requires at least three poles and possibly more complicated singularities.

Nevertheless, the results of the experiments appear surprisingly simple. Above about 1 GeV/c, the  $pp$  total cross section falls smoothly with increasing energy. Also, the differential elastic cross section has a simple  $t$  dependence which also varies smoothly with energy, although exceptions to this smooth energy dependence appear in the form of breaks in the slope of the energy dependence at fixed angles.<sup>1</sup> There is also a more complicated  $t$  dependence emerging in measurements at the highest energies.<sup>2</sup>

Measurements of the polarization in  $pp$  elastic

scattering show first of all that spin effects are not negligible. They also provide a constraint on models which attempt to fit the other physical observables. Polarizations are sensitive to small effects since they come from interference between various helicity amplitudes and we might expect them to show more structure than the cross sections. But below 2 GeV/c and for  $-t < 1$  (GeV/c)<sup>2</sup> at higher momenta, the polarizations have a very simple  $t$  dependence which changes smoothly with energy.

Prior to our work, high-energy polarization measurements have been made for  $-t < 1$  (GeV/c)<sup>2</sup> by Cozzika *et al.*<sup>3</sup> at 1.92 GeV/c; by Neal and Longo<sup>4</sup> at several momenta up to 3.7 GeV/c; by Grannis *et al.*<sup>5</sup> at several momenta between 2.5 and 7.1 GeV/c; and by Borghini *et al.*<sup>6</sup> at 6, 10, and 12 GeV/c. Our results are in general agreement with these other experiments, but extend to larger values of  $-t$ . We do, in fact, see some structure appearing in the  $t$  dependence of the polarizations. More recent results confirm our work and extend our knowledge of the detailed behavior of the  $pp$  polarization to both lower<sup>7</sup> and higher<sup>8</sup> energies.

We have used a polarized proton target together with extensive two-dimensional arrays of scintillation counter hodoscopes and an on-line computer to measure the polarization in the elastic scattering of pions, protons, and kaons from protons. The experiment was carried out at the zero-gradient synchrotron (ZGS) of the Argonne National Laboratory in a secondary beam produced at a target in the external proton beam. Data were re-

corded with beam momenta of 2.50, 2.75, 2.93, 3.25, 3.75, 4.40, and 5.15 GeV/ $c$ . The data acquisition system enabled us to record large numbers of scattering events and to subtract large inelastic backgrounds to obtain statistically significant results even in regions of very low differential cross section. In this paper we present the final results of the measurements for  $pp$  elastic scattering. The  $pp$  results were obtained simultaneously with the measurements from  $\pi^+p$  and  $K^+p$  scattering. The final results for  $K^+p$  and for  $\pi^+p$  and  $\pi^-p$  scattering are presented elsewhere.<sup>9-11</sup> The experimental details are to a great extent common to all the measurements, and in this paper we will give the bulk of the description of the apparatus and the methods by which the polarization data were obtained. A short presentation of our preliminary  $pp$  results at 5.15 GeV/ $c$  has been published.<sup>12</sup>

In Sec. II we describe the apparatus and experimental procedure, and in Sec. III the data analysis. In Sec. IV we present the results of the measurements and point out a few of the features which were either unknown or highly speculative on the basis of previously available data. We fit the  $t$  dependence of the polarizations in terms of a simple model involving a diffractive helicity-nonflip amplitude derived from nearly exchange-degenerate Regge poles. In addition we analyze the energy dependence of all available high-energy polarization data.

## II. APPARATUS

Polarization measurements were carried out by scattering beam particles of a given momentum from a polarized proton target. Scattered particles were detected by crossed arrays of scintillation counters and the information from the counters was processed by an on-line computer and stored for further analysis. Events from elastic scattering off free protons in the polarized target were selected on the basis of coplanarity and kinematic angular correlation. Scattering polarizations were determined by making sets of two runs, one for each direction of target polarization perpendicular to the scattering plane. In the following, we present relevant details of the apparatus and procedures used to obtain the results.

### A. Polarized Proton Target

The polarized proton target used in the experiment was of the lanthanum magnesium nitrate (LMN) type [ $\text{La}_2\text{Mg}_3(\text{NO}_3)_{12} \cdot 24(\text{H}_2\text{O})$ , with 1.5% Nd doping] and has been described elsewhere.<sup>13</sup> A stack of five crystals provided a thickness of 3.7 cm in the direction of traversal by the beam. The

cross-sectional dimensions of the crystals were 2.5 cm horiz. by 1.8 cm vert. The range of the recoil proton and its multiple Coulomb scattering in the target placed a lower limit of about 0.2 (GeV/ $c$ )<sup>2</sup> on the momentum transfer studied.

The target operated at 1.2 °K in a field of 18.6 kG with microwaves of frequency 72 GHz. The magnitude of the polarization of the target  $P_T$  was measured by the usual nuclear magnetic resonance (NMR) method.<sup>14</sup> The method has been checked by observing the polarization in  $pp$  elastic scattering at beam momenta and scattering angles for which the polarization in the scattering is already known from double-scattering experiments.<sup>15</sup> Periodic checks of the calibration constants used in the target polarization analysis were made using the thermal equilibrium polarization produced by the magnet without microwave enhancement. During the course of the experiment, the target polarization varied from 0.40 to 0.60 and averaged about 0.55. The error in the determination of the target polarization is estimated to be  $\pm 0.10$  times the measured value.

The sign of the enhancement of the target polarization was reversed by changing the value of the magnetic field by about 30 G. A correction was applied to the measured scattering polarization for the small geometrical asymmetry resulting from the change in particle trajectories. This correction was in all cases smaller than 0.004 in the polarization for proton-proton scattering.

### B. Secondary Beam

Figure 1 shows the layout of the beam used in the experiment. The secondary beam was produced from a copper target placed in the external proton beam (EPB I) of the ZGS. The intensity of EPB I and the uniformity of the 400-msec-long spill were monitored with a helium-filled ion chamber. Various counter rates were monitored and automatically normalized per unit ion chamber to provide a check of targeting efficiency of EPB I and of the transport efficiency of the secondary beam line. A three-counter telescope, viewing the production target, was used to check the positioning and focusing of EPB I by comparing its counting rate with the ion chamber current.

As indicated in Fig. 1, two bending magnets placed in EPB I were used to extract secondaries produced at 0°. The experimental beam line had two foci, with momentum dispersion at the first and subsequent recombination at the final focus. Quadrupole doublets were used for the focusing lenses, and a quadrupole triplet acted as a field lens. Except for the regions in the beam line occupied by counters, helium bags were placed in

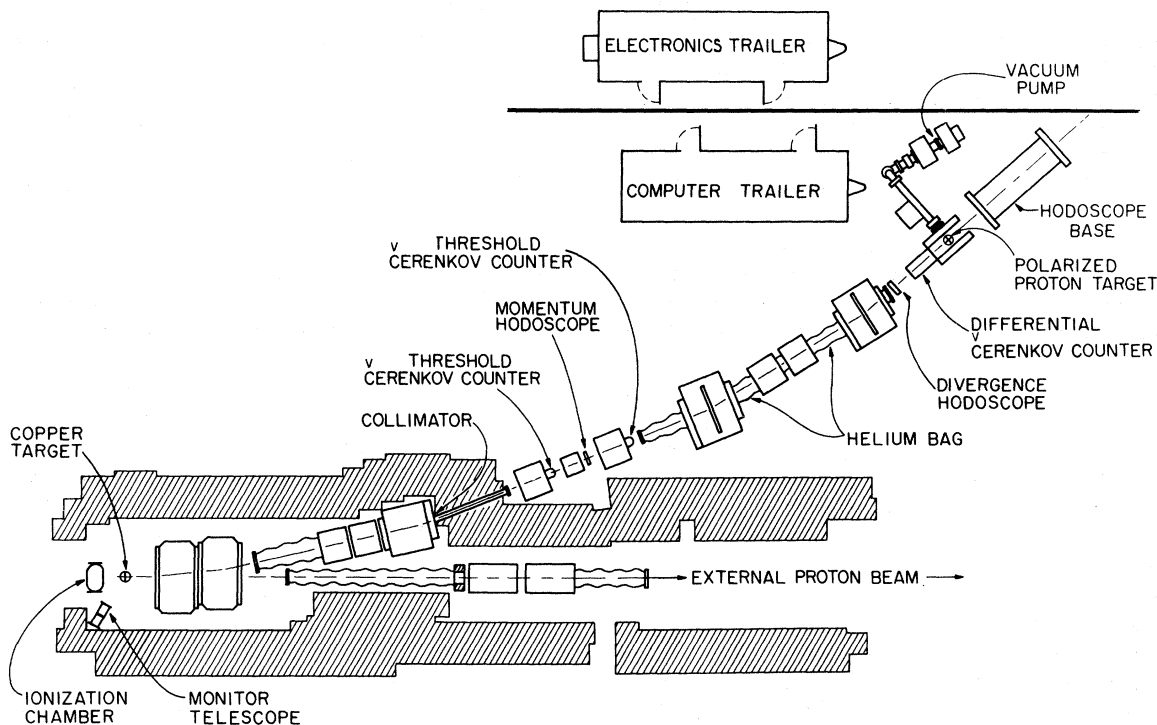


FIG. 1. Diagram of the beam layout. The first focus is at the momentum hodoscope and the second at the position of the polarized proton target.

the entire 40-m length of the beam line to reduce multiple scattering.

For particles having the nominal beam momentum the angular acceptance at the production target was  $\pm 16$  mrad vert. and  $\pm 8$  mrad horiz. The effective solid angle was determined by the apertures of the quadrupole magnets of the first lens. The magnifications in both planes were calculated to be unity at the polarized proton target neglecting aberrations and multiple scattering. The measured spot size for particles with the central momentum was about 1.3 cm vert. by 2.0 cm horiz.

To make efficient use of the intensity-limited external proton beam, a momentum spread of  $\pm 3.5\%$  was accepted by the beam optics. Since the momentum dependence of the polarization was not known, a seven-counter hodoscope was placed at the intermediate focus where the beam was dispersed in momentum. The calculated momentum resolution of the optical system was approximately  $\pm \frac{1}{2}\%$  at the extreme momenta and slightly better for the central momentum. The solid-angle acceptance was smaller for momenta other than the nominal value, and due to chromatic aberration in the optical system the beam-spot size at the polarized proton target was somewhat larger. With the usual  $\Delta p/p$  acceptance of  $\pm 3.5\%$ , the spot size at the target was 2.0 cm vert. and 2.5 cm horiz. The resolution and dispersion of the beam line

were tested by operating EPB I at reduced energy (and intensity) and by selecting monoenergetic protons from elastic  $pp$  scattering off a  $\text{CH}_2$  target. For this, a scintillation counter was placed near the production target at the appropriate angle to tag the elastically scattered protons.

A two-dimensional ( $6 \times 6$ ) hodoscope (labeled divergence hodoscope in Fig. 1) located 310 cm upstream from the final focus, together with another two-dimensional ( $6 \times 8$ ) hodoscope (position hodoscope, see Fig. 2) 50 cm upstream from the target, determined the vertical and horizontal angles of each incident particle and the point where it entered the target.

### C. Beam Particle Identification

Beam particles were classified as electrons, pions, kaons, protons, or "undefined" depending upon the signals from the various Čerenkov counters. The electron signal was generated by a gas threshold Čerenkov counter located just upstream from the intermediate focus. This signal was used as a veto in the fast logic, thus preventing further analysis of any resulting scattering event. It was extremely important to eliminate electrons from the beam because, in the polarized proton target, bremsstrahlung and subsequent pair production generated a large number of coplanar

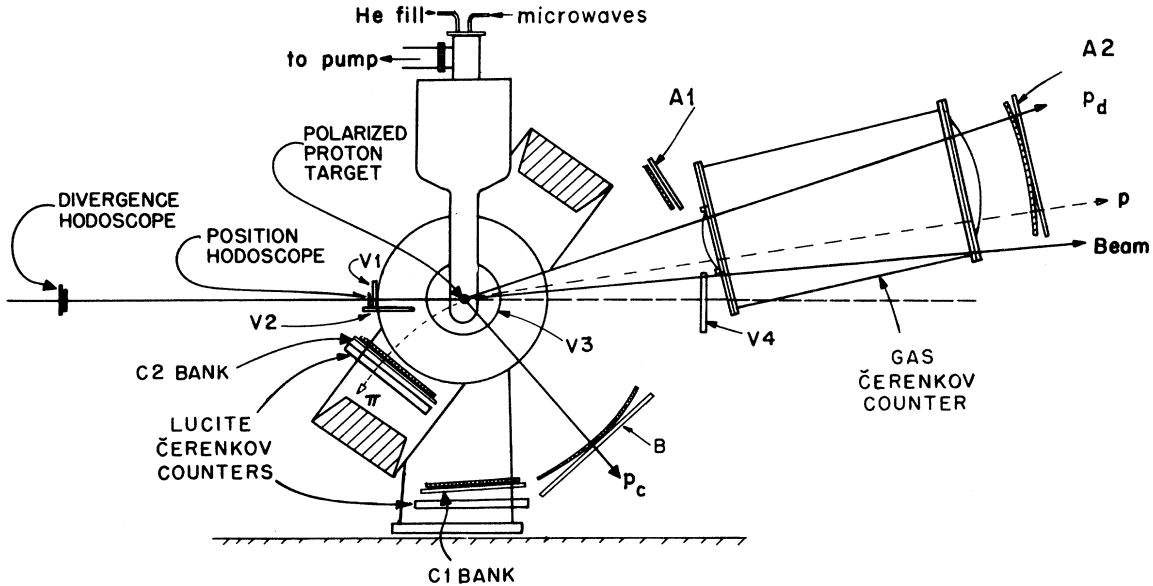


FIG. 2. Plan view showing apparatus used to detect  $pp$  elastic scattering events. The incoming beam is defined by the divergence and position hodoscopes. Elastic  $pp$  scatterings in the near-vertical plane are detected by the crossed arrays (or banks) of counters A1, A2, and B; the solid lines  $p_c$  and  $p_d$  indicate a typical scattering event. Counters V1–V4 were in anticoincidence to reject background. The large gas Čerenkov counter and the C hodoscopes were used in the measurements of backward  $\pi p$  elastic scattering indicated by the dashed lines.

events. This electron counter was more than 98% efficient at all momenta studied and vetoed fewer than 2% of the pions in the beam.

Except when  $K^+$  data were also being taken, the pions were defined by a second gas threshold Čerenkov counter located just downstream from the intermediate focus. Its efficiency for counting pions was greater than 98% for all beam momenta used. Muons in the beam were counted as pions.

A differential Čerenkov counter  $C_3$  with two concentric rings of photomultipliers served to separate  $K^+$ 's from  $\pi^+$ 's in positively charged beams for runs at 3.75 and 4.40 GeV/c. This counter, which has been described elsewhere,<sup>16</sup> provided a kaon signal with a pion contamination of less than 1% and also a pion signal. Protons were defined by no signal in any of the beam Čerenkov counters. Undefined particles were those which triggered either the pion threshold counter or the pion ring of  $C_3$ , but not both. Such incident particles were scaled as a check during the experiment and constituted less than 2% of the beam.

A clearly identified incident particle was thus defined by coincident signals from a timing counter (located adjacent to the momentum hodoscope), all five beam hodoscopes, and various Čerenkov counters according to the mass of the particle. Approximately  $10^6$  such clearly identified incident particles were handled in each ZGS spill. For positive beams the pion to proton ratio ranged

from 1:1 at the lower momenta to 1:3 at the highest momentum.

Fractional rates were scaled and monitored during the collection of data. Such rates displayed the yield of secondaries, the transmission to various points along the beam line, and the constitution of the beam in terms of particle type, momentum, position, and divergence distributions. Most of the observed rates were scaled for a given number of clearly identified incident beam particles and were constant in time to within statistical fluctuations.

#### D. Detection of Scattering Events

Shown in Fig. 2 are the hodoscopes used to detect the scattering events. Each of the hodoscopes A1, A2, and B contained crossed arrays of counters to measure both the polar ( $\theta$ ) and azimuthal ( $\phi$ ) angles of each of the outgoing particles.<sup>17</sup> The hodoscopes labeled C1 and C2, and the large gas Čerenkov counter, were used for measurements of backward  $\pi^+p$  scattering<sup>10</sup> and will not be discussed here. The solid trajectories labeled  $p_d$  and  $p_c$  in Fig. 2 illustrate a typical  $pp$  scattering event. In our treatment of such events, the outgoing particle detected in the A hodoscopes was regarded as "defining" and the one in B as its "conjugate." Knowing the momentum and mass of the incident particle and the angles  $\theta$  and  $\phi$  for the defining

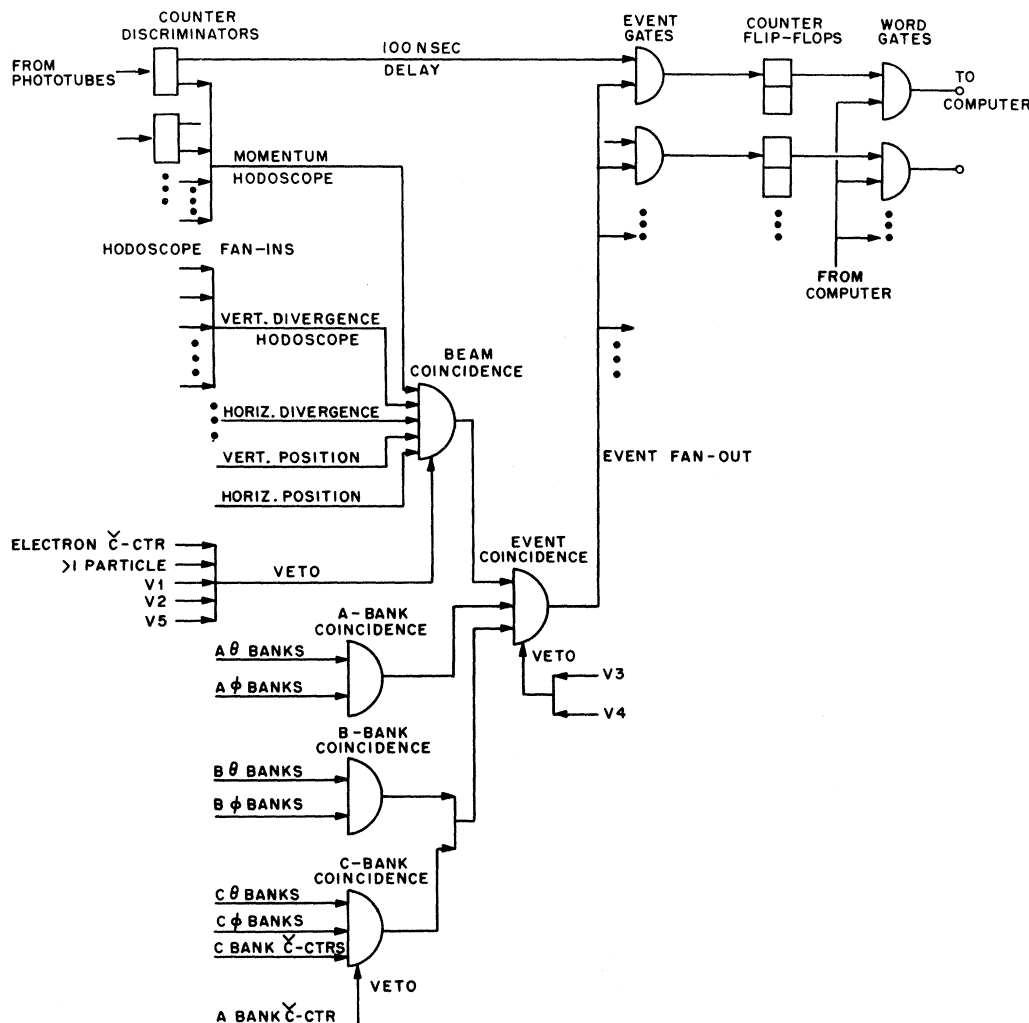


FIG. 3. Schematic diagram of the logical requirements placed on a scattering event before it was transmitted to the computer.

particle, the expected  $\theta$  and  $\phi$  angles for the conjugate particle can be calculated. These kinematic constraints were used to separate elastic scattering events on free protons from the very large inelastic background.

Scintillation veto counters were positioned in the vicinity of the polarized target to eliminate various types of background events. Two veto counters,  $V1$  and  $V2$ , defined an aperture near the position hodoscope and prevented the detection of charged particles scattered from that hodoscope. Another pair of counters,  $V3$ , vetoed background events in which a charged particle entered or left the pole tips of the polarized proton target magnet. When the differential counter was in the beam between the divergence and position hodoscopes, another veto counter,  $V5$ , was installed to shield the target area from the beam particles scattered in its

windows or filling gas. A very important veto counter,  $V4$ , was placed in the beam line downstream from the polarized proton target. This counter reduced the background due to low-momentum-transfer events on complex nuclei in the target.

#### E. Electronic Logic

High-speed electronic logic was used to select those events which were to be transmitted to the computer. A schematic diagram of the logic is shown in Fig. 3. The requirements for a valid event were that (1) one and only one counter in each of the five beam hodoscopes be triggered; (2) signals from the electron Čerenkov counter and all geometry defining veto counters be absent; (3) one  $\theta$  and one  $\phi$  array above the beam, and one  $\theta$  and  $\phi$  array below the beam, be triggered. A

further veto signal was generated in the following way in order to avoid accidentals and incident particle misidentification: Whenever a second trigger occurred in any counter in any beam hodoscope within 24 nsec after another signal in that same hodoscope, a veto signal was generated with timing such that neither beam particle was considered valid. Thus every valid beam particle was preceded and followed by a 24-nsec period during which no other signals were generated in the beam counters. The effect of this technique was to make the measurements to a large extent independent of intensity, and to ensure accurate classification of particle types.

Whenever the electronic requirements for an event occurred, the event coincidence signal was sent to a set of twofold coincidence units, one for each hodoscope counter, and used to gate the individual counter signals into their respective flip-flops. During the decision-making process, the signals from the counters were stored in coaxial cables with propagation delays of 100 nsec.

#### F. On-Line Computer

The fast logic and the gated flip-flops were interfaced to an on-line computer (EMR 6020) by means of word gates and the priority-interrupt features of the computer. When the fast-logic requirements for a scattering event were satisfied, nine words of 24 bits each were gated sequentially onto a word bus to the computer's buffered input/output channel. The fast logic was gated off during the transmission of an event to the computer, whenever the input buffer was full, and at any other time when the computer was unable to accept a new event.

At the end of each beam spill the computer interrogated several scalars. Two of the scalars contained the normalized rates for an individual counter in the vertical position hodoscope and an individual counter in the horizontal position hodoscope. These rates updated a display of the current beam profile. Other scalars contained overall rate information such as the number of counts in the monitor telescope. Some contained normalized rate information such as the number of particles hitting the momentum hodoscope during the time required to collect  $10^6$  valid beam particles.

The programs and displays available on line are described in Sec. III C. The most important function of the on-line computer was to facilitate accurate and rapid checks on the operation and performance of the apparatus. The high reliability thus obtained was essential in the measurement of small asymmetries in low cross sections.

Typical runs lasted 4–6 hours, after which the

target cryostat was refilled with helium and the sign of the target polarization reversed. A typical run resulted in approximately one million events and filled one magnetic tape. Approximately 300 such tapes were accumulated during the experiment.

### III. DATA ANALYSIS

Because the target consisted of only 3% free protons, the chief task in the reduction of the data was to separate the elastic events from the inelastic background, which was principally due to quasi-elastic scattering from nucleons within the complex nuclei of the target crystals. We first describe the general method by which this was done, and then in subsequent subsections give a more detailed and chronological description of the data analysis.

#### A. Separation of Elastic Events

For each two-body event the computer used two-body kinematics and the observed values of the angles  $\theta$  and  $\phi$  of the particle striking the defining array to calculate the expected  $\theta$  and  $\phi$  angles of the conjugate particle. It then formed the quantities  $\Delta\theta$  and  $\Delta\phi$ , which were the differences between the calculated and the observed angles of the conjugate particle. For each bin in the defining  $\theta$  array, three distributions were formed using the angles  $\Delta\theta$  and  $\Delta\phi$ . First the events were distributed in  $\Delta\phi$  and classified as coplanar or noncoplanar, as defined by  $\Delta\phi$  cuts calculated by a Monte Carlo program. This classification was then used to form separate coplanar  $\Delta\theta$  and noncoplanar  $\Delta\theta$  distributions. Elastic events appear as a peak in the coplanar  $\Delta\theta$  distribution as shown in Fig. 4.

Two methods were used to determine the amount of background beneath the peak. The first method used the noncoplanar  $\Delta\theta$  distributions. Since one does not expect appreciable correlation between  $\Delta\theta$  and  $\Delta\phi$  for an inelastic event, the coplanar and noncoplanar  $\Delta\theta$  distributions should have the same shape, apart from the elastic contribution. Hence the noncoplanar  $\Delta\theta$  distributions outside the elastic region (also given by cuts from the Monte Carlo program) were normalized to the coplanar  $\Delta\theta$  distributions to obtain a determination of the background inside the  $\Delta\theta$  cuts.

The second method used to determine the background was simply to fit a polynomial to each coplanar  $\Delta\theta$  distribution outside the  $\Delta\theta$  cuts, and interpolate the result beneath the elastic peak. An example of such a fit is shown in Fig. 4. The actual fit was made to the sum of the coplanar  $\Delta\theta$  distributions for positive and negative target polarization data. The polynomial coefficients de-

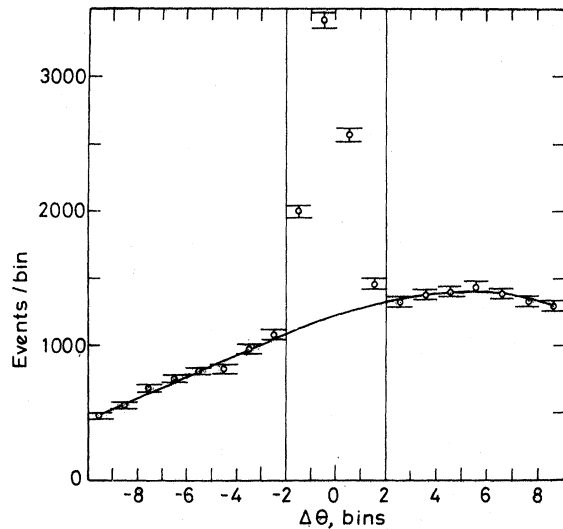


FIG. 4. Graph of the conjugate distribution for a typical defining counter as used in the polynomial background fitting technique. The vertical lines show the locations of the  $\theta$  cuts. Each  $\Delta\theta$  bin is about  $1.5^\circ$  lab angle.

terminated this way and the incident beam intensities for positive and negative runs were used to make the subtractions from the positive and negative data, respectively.

No serious attempt was made to extract differential cross sections from the free-proton scattering rates as has been done in some previous experiments.<sup>15</sup> Apart from the difficulties due to nuclear absorption and multiple scattering in the target and bending of the trajectories in the polarized target magnetic field, there are two effects which make cross-section determinations unreliable. First, the beam spot size was comparable to the target dimensions, and estimates of the fraction of the beam hitting the target are unreliable. However, this effect is mainly one of over-all normalization. A second effect comes from our method of applying cuts in coplanarity and angular correlation. In some cases this results in a loss of elastic events but with a substantial gain in signal-to-background ratio. Nevertheless, the  $t$  distributions of the rates are in qualitative accord with published differential cross section results.

Knowing the relative counting rates  $R^+$  and  $R^-$  (per incident beam particle) for scattering from the free protons, one can then calculate the scattering polarization  $P(t)$  as

$$P(t) = \frac{R^+(t) - R^-(t)}{P_T^+ R^+(t) + P_T^- R^-(t)}, \quad (1)$$

where the superscripts  $\pm$  refer to the direction of the target polarization<sup>18</sup> and  $P_T^\pm$  are the magnitudes of the target polarizations.

### B. Monte Carlo Program

To originally establish the relationship of the conjugate to the defining bins to be used by the on-line programs, the effects on the incident and scattered particle trajectories due to the magnetic field and energy loss in the target were first calculated off line. Next corrections were calculated to account for the beam finite size and divergence as measured by the beam hodoscopes. Such corrections were made to  $\phi$  to account for the horizontal position and slope of the incident particle trajectory, and corrections were made to  $\theta$  to account for the vertical components of the beam particle trajectory, its deviation from the central beam momentum, and the value of  $\cos\phi$  of the scattered particle. (The last correction was necessary since the counter arrays had a cylindrical geometry, whereas the polar angle was the relevant quantity.) A large number of free proton events were then generated by a Monte Carlo program which took into account the finite size, divergence, and momentum spread of the beam, the nonuniform magnetic field, the finite size of the target, and multiple scattering in the cryostat and target. These events were then used to generate  $\Delta\theta$  and  $\Delta\phi$  distributions in the same manner as would be done by the on-line program. Preliminary  $\Delta\theta$  and  $\Delta\phi$  cuts were made on the basis of these distributions, and punched onto cards, along with the kinematics and correction coefficients for each  $\theta$  bin.

### C. On-Line Data Handling

A variety of programs were prepared for the EMR 6020 computer (with 16K memory) used in the experiment. These were stored on magnetic tape as links of a master-chain program. Each link could be summoned manually (through a push-button interrupt) or by any other link.

The normal run sequence began with a link which assisted in tuning the beam. The fast logic was modified to trigger on beam particles alone, rather than on scattering events, and the beam hodoscope information was used to form a variety of beam distributions which could be displayed on a CRT to verify that the beam was properly focused and positioned. For each momentum bin, a matrix of the horizontal-vertical intensity distribution at the target was written onto magnetic tape for subsequent analysis with the scattering data.

The second link read a deck of cards containing input information for the data-taking link such as kinematics, correction coefficients, and cuts. With this information saved in a common area of memory, the data-taking link was called in and the computer was ready to accept events.

The data-taking link withdrew event information from an input buffer, and rejected events in which more than one particle was detected above or below the beam. The remaining two-prong events were encoded into a more compact three-word format and buffered onto magnetic tape. When up to date in the encoding process, the computer analyzed events, applying corrections to the values of  $\theta$  and  $\phi$  and forming the  $\Delta\theta$  and  $\Delta\phi$  distributions as described previously. Although the computer had time to analyze all of the incoming events, storage limitations required that only one type of beam particle (usually pions) be analyzed on line. CRT displays of the  $\Delta\theta$  and  $\Delta\phi$  distributions were available for any of the defining  $\theta$  bins. Additionally, one could display the uncorrelated distribution of counts in any of the arrays or beam hodoscopes, from which noisy or inefficient counters could be quickly detected. By the use of scaler information read between ZGS pulses, continuously updated (as opposed to cumulative) displays of the beam distribution at the position hodoscope enabled one to keep close watch on the beam position.

Additional program links were executed at the end of each run to summarize and plot the accumulated data, and a final link analyzed the polarized proton NMR data, which had been punched onto paper tape every 15 min during a run. In addition to the links just discussed, which were used for every run, additional links were available which enabled one to combine the results of several runs, calculate preliminary polarization values, or display the results of previous runs on the CRT.

#### D. Off-Line Data Reduction

Because the computer could store on-line distributions for only one kind of beam particle and for all momentum bins combined, and because it was desired to adjust some of the  $\Delta\phi$  cuts, the data were reanalyzed from the magnetic tape. The analysis was the same as was done on line except that the momentum hodoscope information was used to break the total 7% momentum bite into three separate regions.

A consistency program was then used to check all the runs used in the final analysis. For each run and each defining  $\theta$  bin, this program summed the total number of events in each of six regions, depending on whether they were inside or outside the  $\Delta\theta$  or  $\Delta\phi$  cuts of the three distributions ( $\Delta\phi$ , coplanar  $\Delta\theta$ , and noncoplanar  $\Delta\theta$ ). For each incident momentum, the total event rates in each region were tabulated on a run-by-run and counter-by-counter basis. Values of  $\chi^2$  were calculated for each counter and each run to give a measure of its agreement with the average of all the runs. In this

way the large backgrounds inherent in the experiment provided a sensitive check of the beam normalization, and any errors or inconsistencies occurring in either the data taking or the data analysis could be readily detected.

#### E. Discussion of Systematic Errors

In addition to the statistical counting errors, the calculated polarization is affected by errors in the determination of the target polarization, beam normalization, background subtraction, beam contamination, and possible variations in counter efficiency.

The polarized target used in this experiment and the method of determining the target polarization<sup>14</sup> have been used in several previous experiments and are believed to be reasonably well understood. In two of the previous experiments,<sup>15</sup> the measured target polarizations were checked by measurements of  $pp$  polarizations at energies for which data exist from double scattering experiments. The relative error in the target polarization  $\delta P_T/P_T$  is estimated to be  $\pm 10\%$ . This results in absolute errors in our measured polarizations of typically  $\pm(0.01-0.03)$ . (We note that this error does not affect the shape of the  $t$  dependence of the polarization, but only the over-all normalization.)

Errors in beam normalization due to accidental coincidence or dead times in the electronics were negligible because of the electronic requirement that valid beam particles be separated by at least 24 nsec. Because the beam spot was larger in size than the target, the principal error in beam normalization was due to drifts in the horizontal position of the beam at the target. Comparison of the backgrounds by the consistency checking program showed the run-to-run beam normalizations to be consistent to within 2%. Because the data were matched in time in pairs of runs of opposite target polarization, the drift error often canceled out, so that the net normalizations between positive and negative target polarizations were found to be consistent to within 1%. In principle the changes in normalization could have been calculated using the beam hodoscope information to compare the target position data of the scattering events with the intensity map of the beam taken between runs. However, in view of the smallness of the correction, it was decided to use the correction factor calculated by the consistency checking program. The goodness of the "consistency  $\chi^2$ " given by the program after the correction factors were applied gives us confidence that the differences between runs were simply in the over-all beam normalization. No evidence of drifts in hodoscope efficiency was found by the program.

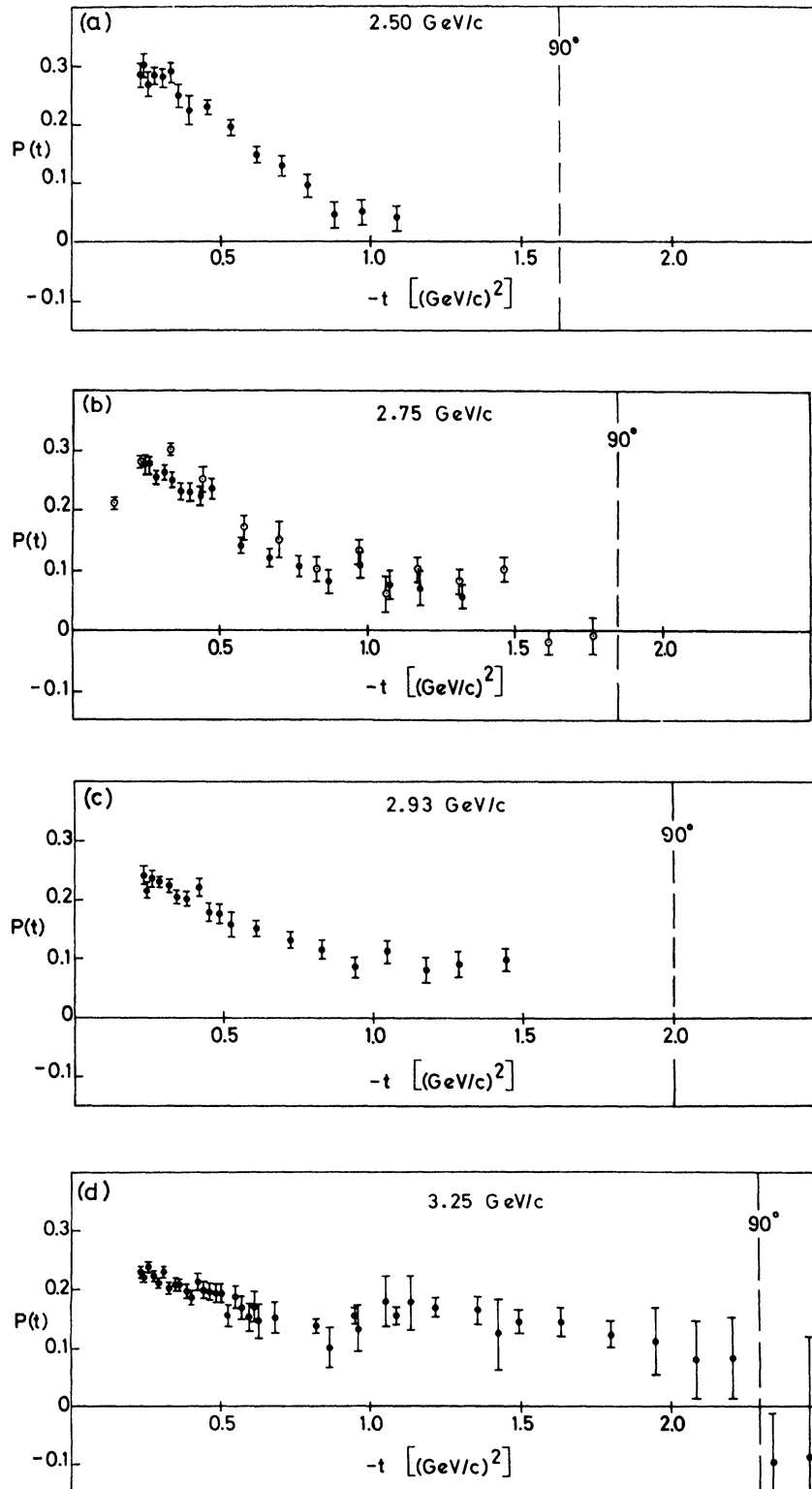


FIG. 5 (Continued on following page).

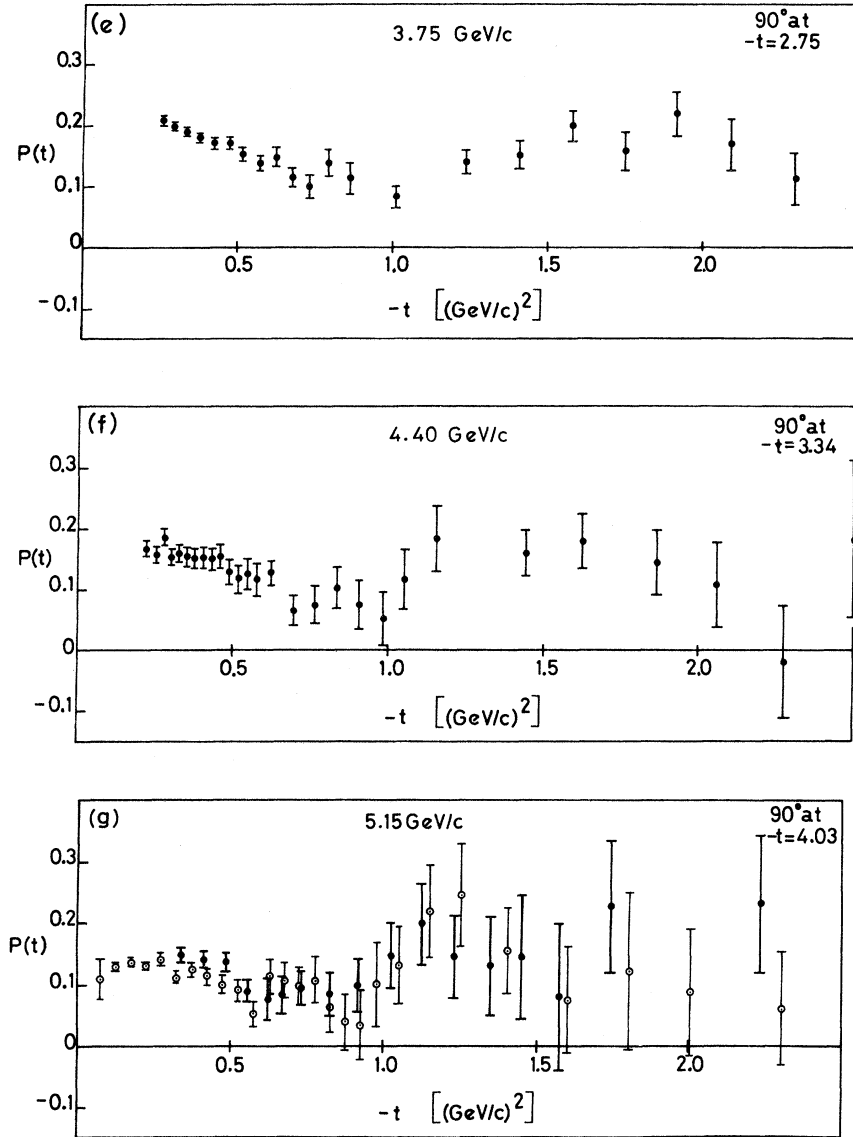


FIG. 5. Polarization results in  $pp$  scattering at (a)  $2.50 \text{ GeV}/c$ , (b)  $2.75 \text{ GeV}/c$ , (c)  $2.93 \text{ GeV}/c$ , (d)  $3.25 \text{ GeV}/c$ , (e)  $3.75 \text{ GeV}/c$ , (f)  $4.40 \text{ GeV}/c$ , and (g)  $5.15 \text{ GeV}/c$ . The closed circles are the results from the present experiment. For comparison purposes we show as open circles in (b) results at  $2.74 \text{ GeV}/c$  from Ref. 7, and in (g), results at  $6 \text{ GeV}/c$  from Ref. 8.

Since the uncorrected data were consistent to within 1%, we may reasonably assume the corrected data were consistent to  $\pm 2\%$ . This results in errors in the polarization of roughly  $\pm 0.01$ .

The polarization results calculated using the two different methods of background subtraction were in good agreement in almost all cases. However, in some cases the noncoplanar background had a different shape from the coplanar background and therefore did not lead to a reliable subtraction. Consequently the polynomial fitting was felt to be the more reliable of the two methods and was the

method used to obtain the final results. The systematic error due to uncertainty in the shape of the background is included in the calculation of the statistical error. The results also proved to be quite insensitive to changes in the cuts.

Pions and kaons constituted less than 2% each of the beam particles classified as protons at all energies. Because  $\pi^+p$ ,  $K^+p$ , and  $pp$  polarizations all have the same sign, and because  $pp$  elastic cross sections are larger than those for  $\pi^+p$  or  $K^+p$ , the resultant error in the polarization is less than 0.01. Electrons and muons constituted a

TABLE I. Measured values of the polarization in elastic proton-proton scattering.

Momentum (GeV/c)	$-t$ [(GeV/c) <sup>2</sup> ]	Polarization	Error	Momentum (GeV/c)	$-t$ [(GeV/c) <sup>2</sup> ]	Polarization	Error	
2.50	0.233	0.282	0.021	3.75	0.259	0.239	0.009	
	0.245	0.299	0.021		0.277	0.224	0.009	
	0.257	0.269	0.021		0.291	0.211	0.009	
	0.278	0.282	0.015		0.309	0.230	0.009	
	0.303	0.279	0.016		0.328	0.203	0.010	
	0.331	0.287	0.017		0.350	0.210	0.011	
	0.358	0.247	0.020		0.362	0.208	0.011	
	0.393	0.225	0.025		0.389	0.197	0.012	
	0.452	0.228	0.013		0.402	0.186	0.012	
	0.531	0.193	0.013		0.421	0.213	0.014	
	0.618	0.147	0.014		0.442	0.200	0.014	
	0.701	0.128	0.017		0.463	0.196	0.015	
	0.789	0.094	0.020		0.483	0.194	0.016	
	0.877	0.045	0.022		0.504	0.194	0.016	
	0.969	0.049	0.022		0.525	0.156	0.018	
	1.084	0.038	0.021		0.548	0.187	0.019	
	2.75	0.245	0.276		0.016	0.571	0.169	0.020
		0.258	0.275		0.015	0.595	0.153	0.023
0.280		0.255	0.011	0.612	0.172	0.025		
0.310		0.263	0.012	0.627	0.146	0.029		
0.338		0.251	0.013	0.679	0.152	0.026		
0.367		0.233	0.014	0.818	0.137	0.012		
0.398		0.230	0.015	0.864	0.102	0.034		
0.432		0.224	0.016	0.947	0.156	0.014		
0.472		0.236	0.017	0.958	0.135	0.039		
0.572		0.141	0.013	1.049	0.180	0.042		
0.669		0.122	0.015	1.086	0.155	0.015		
0.768		0.108	0.017	1.132	0.178	0.047		
0.867		0.082	0.019	1.216	0.169	0.017		
0.976		0.109	0.021	1.355	0.163	0.019		
1.076		0.077	0.024	1.422	0.124	0.060		
1.178		0.071	0.029	1.494	0.146	0.020		
1.320		0.057	0.018	1.631	0.146	0.023		
2.93		0.232	0.242	0.015	1.799	0.124	0.022	
	0.245	0.217	0.013	1.948	0.111	0.056		
	0.260	0.236	0.014	2.083	0.081	0.067		
	0.284	0.231	0.009	2.206	0.085	0.069		
	0.316	0.224	0.011	2.341	-0.096	0.086		
	0.347	0.205	0.011	2.464	-0.087	0.209		
	0.378	0.202	0.012	2.604	-0.201	0.221		
	0.415	0.222	0.014	0.258	0.207	0.008		
	0.450	0.180	0.015	0.295	0.198	0.008		
	0.487	0.177	0.017	0.334	0.190	0.007		
	0.527	0.158	0.021	0.377	0.179	0.008		
	0.606	0.152	0.013	0.423	0.170	0.009		
	0.723	0.132	0.014	0.472	0.170	0.010		
	0.829	0.116	0.016	0.513	0.152	0.011		
	0.938	0.086	0.017	0.574	0.138	0.013		
	1.046	0.111	0.019	0.624	0.148	0.014		
	1.172	0.081	0.020	0.675	0.115	0.016		
	1.286	0.091	0.021	0.732	0.100	0.019		
1.442	0.099	0.019	0.793	0.139	0.022			
3.25	0.232	0.229	0.009	0.862	0.113	0.026		
	0.242	0.221	0.009	1.060	0.083	0.017		
				1.236	0.141	0.019		
				1.404	0.151	0.022		
			1.576	0.198	0.025			
			1.748	0.158	0.030			

TABLE I. (Continued)

Momentum (GeV/c)	$-t$ [(GeV/c) <sup>2</sup> ]	Polarization	Error	Momentum (GeV/c)	$-t$ [(GeV/c) <sup>2</sup> ]	Polarization	Error
	1.910	0.218	0.037		1.863	0.145	0.052
	2.087	0.168	0.042		2.058	0.107	0.070
	2.298	0.113	0.043		2.277	-0.019	0.092
4.40	0.233	0.167	0.013		2.509	0.181	0.129
	0.255	0.156	0.013		2.710	0.010	0.135
	0.278	0.185	0.014		2.960	0.022	0.111
	0.301	0.152	0.013	5.15	0.341	0.148	0.011
	0.326	0.158	0.014		0.411	0.141	0.013
	0.351	0.152	0.015		0.488	0.137	0.015
	0.377	0.150	0.016		0.555	0.090	0.018
	0.403	0.152	0.017		0.625	0.077	0.034
	0.431	0.149	0.018		0.670	0.084	0.029
	0.459	0.153	0.020		0.736	0.095	0.027
	0.488	0.127	0.020		0.825	0.085	0.035
	0.517	0.115	0.022		0.916	0.098	0.043
	0.548	0.125	0.024		1.021	0.147	0.053
	0.579	0.116	0.026		1.124	0.198	0.065
0.624	0.126	0.020	1.232		0.145	0.066	
0.696	0.065	0.024	1.349		0.131	0.080	
0.765	0.075	0.030	1.451		0.145	0.100	
0.838	0.102	0.034	1.574	0.080	0.119		
0.906	0.075	0.040	1.740	0.227	0.106		
0.985	0.052	0.044	2.234	0.231	0.112		
1.051	0.116	0.050	2.800	0.128	0.154		
1.157	0.183	0.053	3.333	0.131	0.145		
1.445	0.158	0.037	3.736	-0.037	0.275		
1.627	0.178	0.043	4.055	-0.214	0.279		

small fraction of the beam. Also, muons have a negligible cross section for elastic scattering, and electrons would contribute only background rather than elastic events.

#### IV. RESULTS AND DISCUSSION

##### A. Experimental Results

The experimental results are presented in Fig. 5 and are also listed in Table I. The data from each of the seven momentum bins were added together since no momentum dependence was found at one momentum which was inconsistent with the gradual tendencies shown by the data. At 2.50 GeV/c we see the feature which has been noticed before<sup>19</sup> at momenta above about 1.9 GeV/c, namely, that the polarization becomes small in the vicinity of  $-t=1$  (GeV/c)<sup>2</sup>. The earlier measurements suggested that when the point  $-t=1$  moved into the physical region as the energy is increased, the polarization lost its characteristic  $\sin\theta\cos\theta$  shape and remained close to zero beyond  $-t\approx 1$ .

However, our results show that at higher momenta the polarization increases beyond  $-t\approx 1$  up to a value of about 0.2. A minimum in the value of the polarization at  $-t\approx 0.8$  to 1 (GeV/c)<sup>2</sup> is clearly evident at nearly all momenta. The results at all momenta appear to be consistent with the dip-secondary-bump structure characteristic of the data at 3.25 GeV/c and above; below 2 GeV/c the structure is outside the physical region; at momenta between 2 and 3 GeV/c the secondary bump is suppressed by the  $\cos\theta$  factor which makes the polarization antisymmetrical about 90°, while above 3 GeV/c the  $\cos\theta$  factor has little effect.

At small  $-t$  the maximum of the polarization decreases monotonically with increasing energy from a value of 0.3 at 2.5 GeV/c to 0.15 at 5.2 GeV/c (and down to about 0.05 at 14 GeV/c).<sup>8</sup> However, at larger  $-t$ , say 1.5, the maximum of the polarization at first increases (although this may be largely due to the effect of the  $\cos\theta$  factor mentioned above) to a value of about 0.15 at which it appears to remain between 3.25 and 5.15 GeV/c. The CERN results<sup>8</sup> at 6 GeV/c also indicate a value of about 0.15. However, by 17.5 GeV/c this

value has dropped to 0.07–0.10. Thus, apparently the energy dependence is less marked at large  $-t$  than at small  $-t$ . We note that the differential elastic cross section exhibits just the opposite behavior, i.e., marked energy dependence at large  $-t$  and weaker at small  $-t$ .

The minimum in  $P(t)$  at  $-t \approx 0.8-1$  is possibly related to the shoulderlike structure which develops<sup>1,2</sup> in  $d\sigma/dt$  at  $-t \approx 1$  at momenta above 7 GeV/c. Since  $P$  is proportional to interference terms between various amplitudes, it is possible for structure to show up at lower energies in  $P$  than in  $d\sigma/dt$ . We will discuss this possible connection in more detail later.

### B. Formalism

Before discussing possible interpretations of the results, we will summarize the formalism and assumptions usually used in the analysis of experimental data at high energies. The differential cross section and polarization for  $pp$  scattering may be written<sup>20</sup> in terms of  $s$ -channel helicity amplitudes as

$$\frac{d\sigma}{dt} = \frac{K}{p_L^2} (|\phi_1|^2 + |\phi_2|^2 + |\phi_3|^2 + |\phi_4|^2 + 4|\phi_5|^2) \quad (2)$$

and

$$P = \frac{-2K}{p_L^2} \frac{\text{Im}[(\phi_1 + \phi_2 + \phi_3 + \phi_4)\phi_5^*]}{d\sigma/dt}, \quad (3)$$

where  $p_L$  is the lab momentum and  $K$  is a constant depending upon the normalization and units of the  $\phi_i$ . The amplitudes  $\phi_1$  and  $\phi_3$  correspond to no helicity flip,  $\phi_2$  and  $\phi_4$  to double helicity flip, and  $\phi_5$  to single helicity flip. In order to remove kinematic singularities, Wang<sup>21</sup> has shown that  $\phi_2$  and  $\phi_4$  should contain a factor  $-t/(4m^2)$ , and  $\phi_5$  a factor  $[-t/(4m^2)]^{1/2}$ . This latter factor also ensures that  $P$  vanishes at  $t=0$ .

Because of the factor  $-t$  in  $\phi_2$  and  $\phi_4$ , it is usual to neglect them in discussing results at small values of  $-t$ ; also there is not enough information to determine them.<sup>22</sup> One can reduce the number of amplitudes to two by assuming

$$\begin{aligned} \phi_2 &= \phi_4 = 0, \\ \phi_1 + \phi_3 &= 2\phi_N, \end{aligned}$$

and

$$\phi_5 = [-t/(4m^2)]^{1/2} \phi_F,$$

where  $N$  indicates helicity nonflip and  $F$  indicates helicity flip. Then Eqs. (2) and (3) reduce to

$$\frac{d\sigma}{dt} = \frac{K}{p_L^2} (2|\phi_N|^2 - t|\phi_F|^2/m^2) \quad (4a)$$

and

$$P = \frac{-2K}{p_L^2} [-t/(4m^2)]^{1/2} \frac{\text{Im}(2\phi_N\phi_F^*)}{d\sigma/dt}, \quad (4b)$$

where in Eq. (4a) we also assume<sup>23</sup>  $\phi_1 = \phi_3$ .

Due to particle identity  $\phi_F$  must have a zero at  $90^\circ$  in the c.m. system; this can be accomplished with a factor  $\cos\theta = 1 + t/(2q^2)$ , where  $q$  is the center-of-mass momentum. Also in order to make  $P$  vanish at  $180^\circ$  as well as at  $0^\circ$ , the quantity  $[-t/(4m^2)]^{1/2}$  should be symmetrized. This can be accomplished by replacing  $t$  with  $t^* = tu/s$ . Then the kinematic factor in  $\phi_5$  becomes

$$[-t^*/(4m^2)]^{1/2} \cos\theta = \sin\theta \cos\theta (q^2/m\sqrt{s}),$$

which is reminiscent of the shape of the low-energy polarization data. With these considerations, Eq. (4b) becomes

$$P(t) = \frac{-2K}{p_L^2} \frac{[-t^*/(4m^2)]^{1/2} \cos\theta \text{Im}(2\phi_N\phi_F^*)}{d\sigma/dt}. \quad (5)$$

### C. Models

A wide variety of models have been used to try to interpret or fit high-energy  $pp$  scattering data.<sup>24</sup> In only a few cases have the models attempted to fit polarization data as well as cross sections. Most models have been based upon the Regge-pole exchange model, the eikonal model leading to a multiple-scattering series, or a combination of the two. Fits to the experimental data with Regge poles alone have been rather unsuccessful.<sup>20</sup> In the eikonal model the input or single-scattering term is often taken as the fourth power of the electromagnetic form factor.<sup>25</sup> Although the multiple-scattering series so derived may be satisfactory in the high-energy limit, it appears necessary to add Regge-pole contributions ( $\rho, f^0, \omega, A_2$ ) at presently accessible energies.<sup>26,27</sup> In this case the eikonal model effectively becomes a method of parametrizing Regge cuts. The Regge-pole contributions are usually taken to be exchange-degenerate in the trajectories, and often also in the residues.

One success of the eikonal approach is its ability to qualitatively explain, in terms of rescattering

effects, the shoulder in the  $pp$  differential cross section which develops at  $-t \approx 1$  for momenta above about 7 GeV/c. The model predicts that as the energy increases and Regge exchanges become less important the structure should become sharper, and this appears to be in agreement with experiment. On rather general grounds it is expected that a structure like this in the differential cross section will have associated with it a rapid variation of the polarization with momentum transfer.<sup>28</sup> Among possible mechanisms are diffraction minima, minima produced by interference between rescattering terms, and Regge nonsense zeros.

Some detailed fitting to experimental data with the eikonal model has been performed by Capella *et al.*<sup>27</sup> In their model a diffractive component with no helicity flip is constructed from a multiple-scattering series and the polarization is produced by interference with an helicity-flip term which is dominated by Regge-pole exchange. Their calculations do show some structure in the polarization, mainly in the form of a minimum in  $P$  at  $-t \approx 1$  (GeV/c)<sup>2</sup> which becomes deeper as the energy increases. They use exchange-degenerate  $f$  and  $\omega$  trajectories with some exchange-degeneracy breaking in the helicity-flip residues, and both the rescattering effects in the nonflip amplitude and the exchange-degeneracy breaking in the helicity-flip amplitude contribute to the structure.

Jacob and Weyers<sup>29</sup> have discussed  $pp$  polarizations along the same lines, but in a more qualitative way. They associate a sharp dip at  $-t \approx 0.6$  in the CERN  $pp$  polarization data at 6 GeV/c with the breaking of exchange degeneracy in the helicity-flip amplitude, and further structure at  $-t \approx 1$  with rescattering. Briefly, they assume that  $\phi_F$  is given by the exchange of  $f$  and  $\omega$  Regge poles as

$$\begin{aligned} \phi_F = & \beta_f(t) [1 + e^{-i\pi\alpha_f(t)}] (s/s_0)^{\alpha_f(t)} \\ & + \beta_\omega(t) [1 - e^{-i\pi\alpha_\omega(t)}] (s/s_0)^{\alpha_\omega(t)}. \end{aligned} \quad (6)$$

Assuming exchange degeneracy for the trajectories,  $\alpha_f(t) = \alpha_\omega(t) = \alpha(t)$ , and writing  $B_1 = \beta_f + \beta_\omega$  and  $B_2 = \beta_f - \beta_\omega$ , they obtain

$$\phi_F = [B_1(t) + B_2(t)e^{-i\pi\alpha(t)}] (s/s_0)^{\alpha(t)}. \quad (7)$$

If the residues are also exchange-degenerate, then  $B_2(t) = 0$  and  $\phi_F$  is purely real. Assuming that the polarization is given by the interference of  $\phi_F$  with a diffractive and structureless nonflip amplitude  $i\gamma(t)(s/s_0)$ , they obtain

$$\begin{aligned} P(t) \approx & [-t/(4m^2)]^{1/2} f(t) [B_1(t) + B_2(t) \cos \pi\alpha(t)] \\ & \times (s/s_0)^{\alpha(t)-1}, \end{aligned} \quad (8)$$

where  $f(t) = 2/\gamma(t)$  and the contribution of  $\phi_F$  to  $d\sigma/dt$  has been neglected. The term in  $\cos \pi\alpha(t)$  gives a smooth oscillatory structure of periodicity  $\Delta t \approx 1.2$ , and if  $B_2$  is negative will give a minimum in  $P(t)$  at  $-t \approx 0.6$ .

With an expression such as Eq. (8) it is possible to obtain good fits to the polarization data at individual energies without any rescattering corrections. As an example of this we have fitted with a helicity-flip amplitude which breaks exchange degeneracy linearly in  $t^*$ :

$$\phi_F = (b_1 + b_2 t^* e^{-i\pi\alpha(t)}) (s/s_0)^{\alpha(t)},$$

with  $\alpha = \alpha_0 + \alpha' t^*$ ; we approximate  $\phi_N$  by

$$\phi_N = \{ [p_L^2 / (2K)] d\sigma/dt \}^{1/2}$$

and take  $d\sigma/dt$  from Krisch's fit<sup>30</sup> to cross-section data,  $d\sigma/dt \approx 90 \exp(10t^*)$ . The expression used in fitting is

$$P(t) = \frac{2[-t^*/(4m^2)]^{1/2} \cos \theta [b_1 + b_2 t^* \cos \pi\alpha(t)] (s/s_0)^{\alpha(t)}}{p_L 90^{1/2} \exp(5t^*)} \left( \frac{s}{s_0} \right)^{\alpha(t)}, \quad (9)$$

and in Fig. 6 we show the fit obtained to the data at 4.4 GeV/c with  $\alpha_0$  fixed at 0.5 and  $s_0$  fixed at 0.22 GeV<sup>2</sup>. The values of the adjustable parameters found were  $b_1 = 3.1$ ,  $b_2 = 4.7$ , and  $\alpha' = 0.80$  (GeV/c)<sup>-2</sup>. Similar good fits were found at other momenta but with some changes in the values of the parameters, and data at 4.40, 5.15, and 6.0 GeV/c were fitted simultaneously with  $b_1 = 3.3$ ,  $b_2 = 4.6$ , and  $\alpha' = 0.90$  (GeV/c)<sup>-2</sup> with  $\chi^2/N_{df} = 1.0$ . The  $\alpha'$  found is in good agreement with commonly accepted values for the  $f$  and  $\omega$  trajectories, and the simple model of exchange-degeneracy breaking in  $\phi_F$  qualitatively fits the observed structure. However, this model as outlined above does not give the correct energy dependence.

If  $\alpha$  is written as a linear function of  $t^*$  then Eq. (9) becomes completely symmetric in  $t$  and  $u$  and an acceptable simultaneous fit to the polarization data is found for all values of  $p_L \geq 2.5$  GeV/c.<sup>31</sup>

#### D. Energy Dependence

At present it is difficult to interpret the energy dependence of the polarizations. First of all, the energy dependence of the differential cross section is not well understood, especially as new measurements<sup>1</sup> show that the structure at  $-t \approx 1.2$  (GeV/c)<sup>2</sup> develops very rapidly between 7 and

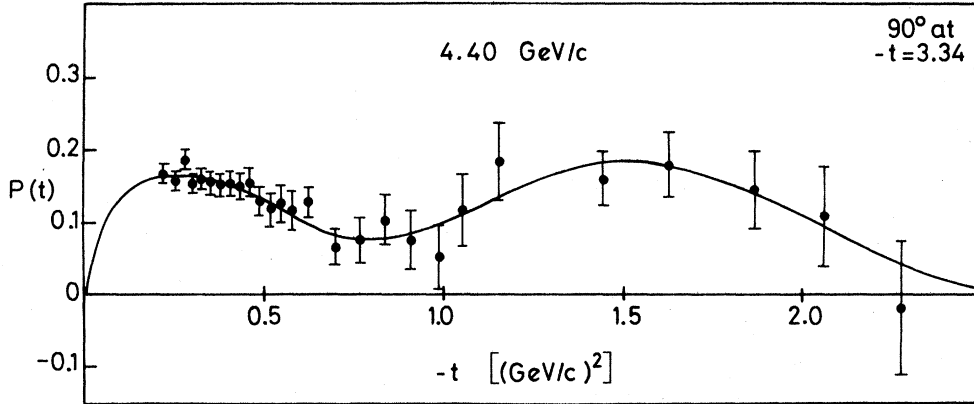


FIG. 6. Sample fit to  $p$ - $p$  polarization data at 4.40 GeV/c with a simple model of exchange-degeneracy breaking. The fitted curve comes from Eq. (9) with parameter values given in the text.

10 GeV/c but changes rather slowly above 10 GeV/c. It is usual to extract the energy dependence of the cross sections with the expression

$$\frac{d\sigma}{d\Omega} = [K(t)/s](\nu/s_0)^{2\alpha(t)}, \quad (10)$$

where  $\nu = \frac{1}{2}(s - u)$ , or equivalently,

$$\frac{d\sigma}{dt} = \frac{1}{p_L^2} f(t) \left( \frac{\nu}{s_0} \right)^{2\alpha(t)}. \quad (11)$$

In these expressions  $\alpha(t)$  gives the energy dependence as a function of  $t$  and may be thought of as the dominant trajectory or, more correctly, the effective trajectory. If there is more than one term in the energy dependence, a plot of  $\ln(p_L^2 d\sigma/dt)$  vs  $\ln(\nu)$  at fixed  $t$  should not be a straight line of slope  $2\alpha$ , but should exhibit some curvature. Considering only data above 7 GeV/c, Pinsky<sup>32</sup> has found that only a single term is required in the range  $2 < -t < 15$ . Nevertheless, the interpretation of the energy dependence is not obvious. If data in the interval 2–7 GeV/c are included, this simple form does not work at some  $t$  values because the cross sections at fixed  $t$  change more rapidly with  $\nu$  at the lower momenta. Recently Kammerud *et al.*<sup>1</sup> have performed a similar analysis on their new data ( $2.7 < p_L < 5.5$ ) in the range  $0.4 < -t < 4.0$ . They find a steeper slope at the same  $t$  value than does Pinsky with the higher-energy data. In Fig. 7(a) we show some plots of  $\ln(p_L^2 d\sigma/dt)$  vs  $\ln(\nu)$  in the  $t$  range relevant to the present experiment. The cross sections were obtained in part from the compilation of Alexander *et al.*<sup>33</sup> and were interpolated to find values at fixed values of  $-t$ . Clearly there is considerable curvature at some  $t$  values. Also, in some cases  $d\sigma/dt$  is not well determined; in some regions there is disagreement between different experiments, and in other regions there are not

enough data points. The curves shown are hand-drawn and were used to interpolate values of  $d\sigma/dt$  in order to calculate values of  $P d\sigma/dt$  discussed below.

If we try to interpret the polarization as being due to interference between a dominant diffractive helicity-nonflip amplitude and a Regge-pole helicity-flip amplitude, then we expect

$$P(t) \propto \left( \frac{\nu}{s_0} \right)^{\alpha_R - \alpha_D}, \quad (12)$$

where  $\alpha_R \approx \frac{1}{2} + t$  and  $\alpha_D \approx 1.0$  for small  $-t$ . This form does not appear to be consistent with the experimental data, as has been shown by Odorico *et al.*<sup>34</sup> and by Albrow *et al.*<sup>7</sup>; the energy dependence of the experimental data is steeper than this.

To exhibit the energy dependence of the polarizations more clearly it is useful to plot  $\ln(\sigma_P)$  vs  $\ln(\nu)$ , where we define  $\sigma_P$  according to

$$\sigma_P \equiv \frac{p_L^2 P(t)}{[-t/(4m^2)]^{1/2} \cos\theta} \frac{d\sigma}{dt}. \quad (13)$$

The quantity  $\sigma_P$  is proportional to the imaginary part of the interference terms, has the obvious kinematic terms included, and in the simple model discussed above should behave like  $(\nu/s_0)^{\alpha_R - \alpha_D}$ . We show such a plot for different values of  $t$  in Fig. 7(b) using not only our polarization data, but also data from other experiments.<sup>3,4,7,8</sup>

For this plot, values of  $d\sigma/dt$  were obtained from the curves drawn in Fig. 7(a), but the errors shown are only the quoted statistical errors in the polarizations. The systematic errors in the polarizations are typically  $\pm 10\%$  for the various experiments; errors in the cross sections are not included. For the  $-t$  values 0.2, 0.4, and 0.8, the quantity  $\sigma_P$  clearly shrinks, and shrinks more rapidly than the cross section does. Note that the

CERN polarization data<sup>8</sup> at high momenta (e.g., 17.5 GeV/c) are needed for obtaining information on the energy dependence; it is difficult to say anything conclusive on the basis of measurements from any single experiment because they span such a small range of  $\nu$ . Of course we need to consider systematic errors in the data at different momenta from the same experiment, and also the strong possibility that there are normalization changes from one experiment to another. The results from our experiment and the CERN work at higher momenta appear to be compatible in normalization; there appear to be normalization problems for some of the experiments at lower momenta. In spite of the systematic errors, the conclusions we make below are not strongly affected by reasonable changes in normalizations. Re-

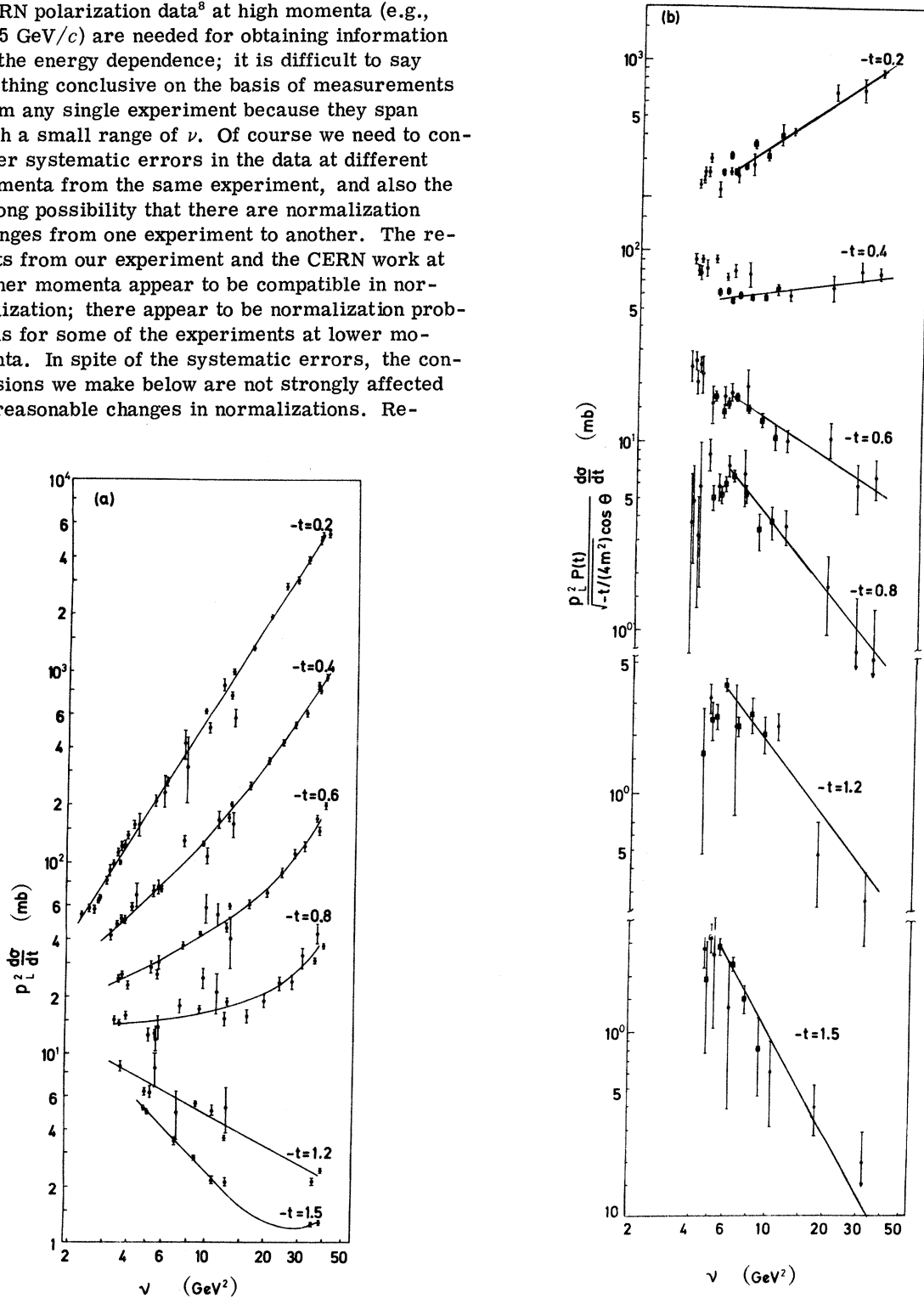


FIG. 7. Plots showing the energy dependence at fixed  $t$  of (a) the unpolarized differential cross sections  $p_L^2 \frac{d\sigma}{dt}$  and (b) the polarized cross sections  $\sigma_P$  in elastic  $pp$  scattering. The lines in (a) are drawn to interpolate for values of  $d\sigma/dt$ . The straight lines in (b) are from fits with Eq. (14). The experimental points come from a large number of experiments; the points marked ( $\blacksquare$ ) are derived from polarization values from this experiment.

turning to Fig. 7(b), at  $-t \approx 1.2$ ,  $\sigma_P$  appears to be rather independent of energy up to 6 GeV/c, and then decreases rapidly. This behavior is probably associated with the development of the shoulder in  $d\sigma/dt$ . At  $-t=1.5$ ,  $\sigma_P$  falls off smoothly with increasing  $\nu$  and at about the same rate as at  $-t=0.8$ . In spite of the apparent nonlinearity of the plot at  $-t=1.2$ , we have fitted the results with  $\nu \geq 5.7$  (GeV)<sup>2</sup> for each value of  $t$  shown with

$$\sigma_P(t) = c(t)(\nu/s_0)^{\alpha_e(t)}. \quad (14)$$

Here  $\alpha_e(t) = (\alpha_D + \alpha_R)_e$  or more generally  $(\alpha_1 + \alpha_2)_e$ , where  $\alpha_1$  and  $\alpha_2$  correspond to the two dominant exchanges responsible for the interference term which produced the polarization. The fitted lines are shown in Fig. 7(b) and the results of the fits are given in Table II.

Without an assumption or a model, it is impossible to extract  $\alpha_1$  and  $\alpha_2$  independently. Also it is very likely that more than one exchange contributes to  $\phi_P$  or  $\phi_N$  and, hence, each of  $\alpha_1$  and  $\alpha_2$  may be the result of several exchanges. A possible assumption is that one of them, say  $\alpha_2$ , comes from Regge pole exchange with the commonly accepted  $\alpha_2 = 0.5 + 0.9t$ . With this assumption

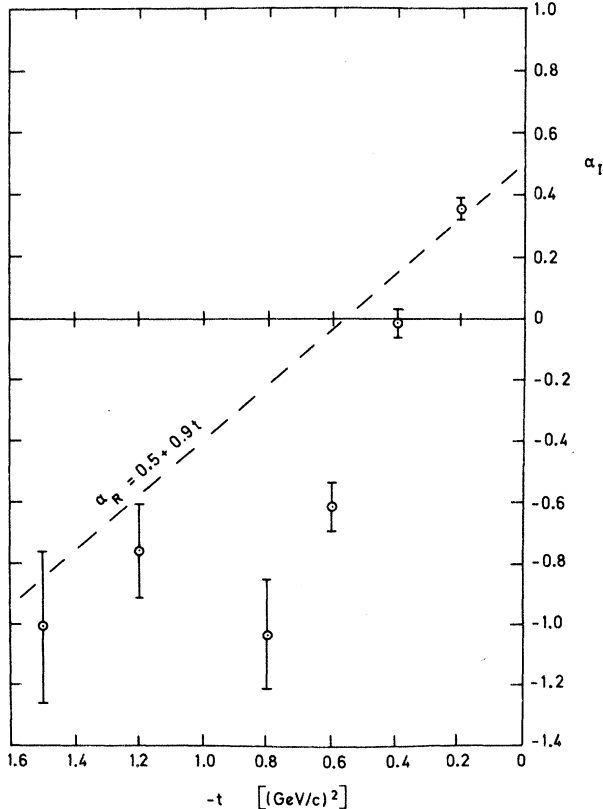


FIG. 8. Plot of  $\alpha_1 = \alpha_e - (0.5 + 0.9t)$  vs  $t$ , where  $\alpha_e$  is derived from fits with Eq. (14).

TABLE II. Energy dependence of  $pp$  polarized cross sections: Results of fits to

$$\sigma_P \equiv p_L^2 \frac{(d\sigma/dt)P(t)}{[-t/(4m^2)]^{1/2} \cos\theta} = c(t)(\nu/s_0)^{\alpha_e(t)}.$$

$-t$ [(GeV/c) <sup>2</sup> ]	$\alpha_e$	$\alpha_R^a$	$\alpha_1^b$	$\alpha_x^c$
0.2	0.68 ± 0.03	0.32	0.36	-0.32
0.4	0.13 ± 0.04	0.14	-0.01	-0.87
0.6	-0.65 ± 0.08	-0.01	-0.61	-1.65
0.8	-1.25 ± 0.18	-0.22	-1.03	-2.25
1.2	-1.34 ± 0.15	-0.58	-0.76	-2.34
1.5	-1.86 ± 0.25	-0.85	-1.01	-2.86

<sup>a</sup> Calculated from  $\alpha_R = 0.5 + 0.9t$ .

<sup>b</sup> Assuming  $\alpha_R = 0.5 + 0.9t$  and  $\alpha_1 = \alpha_e - \alpha_R$ .

<sup>c</sup> Assuming  $\alpha_D = 1$  and  $\alpha_x = \alpha_e - \alpha_D$ .

we have extracted the  $\alpha_1(t)$  listed in Table II and plotted it vs  $t$  in Fig. 8. Now in the simple model which we have discussed above,  $\alpha_1$  should be associated with the diffractive amplitude or with the

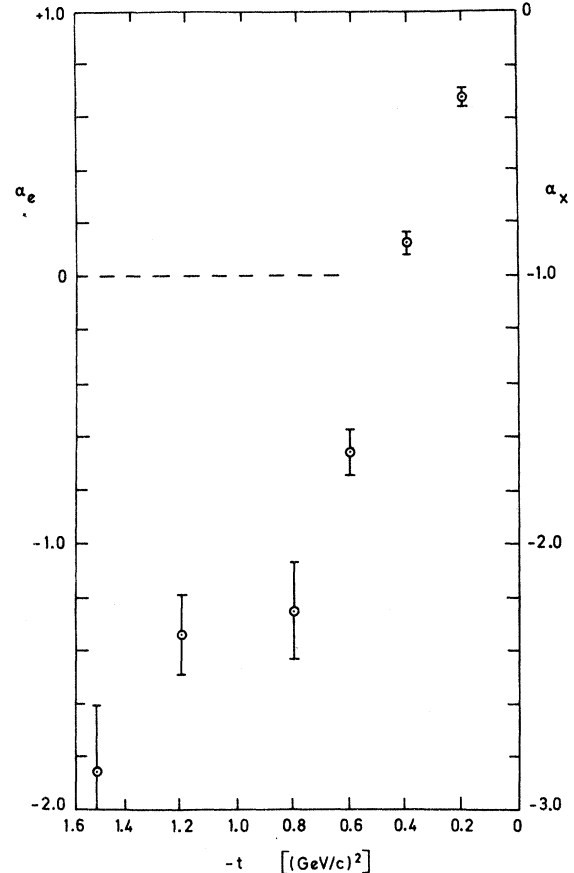


FIG. 9. Plot of  $\alpha_e$  and  $\alpha_x = \alpha_e - 1$ , where  $\alpha_e$  is derived from fits with Eq. (14).

main contribution to the multiple-scattering series, and in particular  $\alpha_1=1$  for  $-t=0$ . This equality is not inconsistent with the results shown in Fig. 8, but the extracted  $\alpha_1$  falls much more rapidly with increasing  $-t$  than we would expect.

Another possibility is to assume that there is a diffractive amplitude with  $\alpha_D=1+\alpha'_D t$ . By subtracting this from  $\alpha_e$  we find the trajectory of the amplitude which interferes with  $\alpha_D$  to produce the polarization. For the case  $\alpha'_D=0$ , we tabulate  $\alpha_x=\alpha_e-\alpha_D$  in Table II and plot it in Fig. 9. The result is a very low-lying trajectory, much lower

than  $\alpha_R$ , and this result does not change appreciably for  $\alpha'_D \neq 0$ .

#### ACKNOWLEDGMENTS

A. Gonis, R. Larson, A. Lesnick, and H. Petri provided valuable assistance during several portions of the experiment. We owe our thanks to the operating staff of the ZGS and the technical staff of the Enrico Fermi Institute for their excellent support. We are particularly indebted to T. Numakura and R. Norton for the design of special electronics used in the experiment.

\*Work supported by the National Science Foundation under Grants No. GP-6135 and GU-2175 and by the U. S. Atomic Energy Commission.

†This work is based on a thesis submitted by James H. Parry in partial fulfillment of the requirements for the Ph.D degree at the University of Chicago.

‡Present address: Computer-Based Education Research Laboratory, University of Illinois, Urbana, Illinois 61801.

§Present address: Nuclear Physics Laboratory, University of Oxford, Oxford, England.

||Present address: Rutherford High Energy Laboratory, Chilton, Didcot, Berkshire, England.

\*\*Present address: Stanford Linear Accelerator Center, Stanford, California, 94305.

<sup>1</sup>J. V. Allaby, F. Binon, A. N. Diddens, F. Duteil, A. Klovning, E. Lillethun, R. Meunier, J. P. Peigneux, E. J. Sacharidis, K. Schlüpmann, M. Spighel, J. P. Stroot, A. M. Thorndike, and A. M. Wetherall, *Phys. Lett.* **28B**, 67 (1968); J. V. Allaby, A. N. Diddens, R. W. Robinson, A. Klovning, J. Litt, L. S. Rochester, K. Schlüpmann, A. M. Wetherall, U. Amaldi, C. Bosio, R. Biancastelli, and G. M. Matthise, *Phys. Lett.* **34B**, 431 (1971); R. C. Kammerud, B. B. Brabson, R. R. Crittenden, R. M. Heinz, H. A. Neal, H. W. Paik, and R. A. Sidwell, *Phys. Rev. D* **4**, 1309 (1971).

<sup>2</sup>See, for example, R. A. Carrigan Jr., R. M. Edelman, N. C. Hien, T. J. McMahon, I. Nadelhaft, E. W. Anderson, E. J. Bleser, G. B. Collins, T. Fujii, J. Menes, and F. Turkot, *Phys. Rev. Lett.* **24**, 683 (1970); R. M. Edelman *et al.*, *Phys. Rev. D* **5**, 1073 (1972); J. V. Allaby *et al.*, *Nucl. Phys. B* (to be published).

<sup>3</sup>G. Cozzika, Y. Ducros, A. de Lesquen, J. Movchet, J. C. Raoul, L. van Rossum, J. Deregél, and J. M. Fontaine, *Phys. Rev.* **164**, 1672 (1967).

<sup>4</sup>H. A. Neal and M. J. Longo, *Phys. Rev.* **161**, 1374 (1967).

<sup>5</sup>P. Grannis, J. Arens, F. Betz, O. Chamberlain, B. Dieterle, C. Schultz, G. Shapiro, H. Steiner, L. van Rossum, and D. Weldon, *Phys. Rev.* **148**, 1297 (1966).

<sup>6</sup>M. Borghini, G. Coignet, L. Dick, K. Kuroda, L. Di Lella, P. C. Macq, A. Michalowicz, and J. C. Olivier, *Phys. Lett.* **24B**, 77 (1967).

<sup>7</sup>M. G. Albrow, S. Andersson/Almehed, B. Bosnjakovic, C. Daum, F. C. Erne, J. P. Lagnaux, J. C. Sens, and F. Udo, *Nucl. Phys.* **B23**, 445 (1970).

<sup>8</sup>M. Borghini, L. Di Lella, A. Navarro, J. C. Olivier, K. Reibel, C. Coignet, D. Cronenberger, G. Gregoire, K. Kuroda, A. Michalowicz, M. Poulet, D. Sillou, C. Bellettini, P. L. Braccini, T. del Prete, L. Foa, G. Sanguinetti, M. Valdata, I. Dick, H. Aoi, and Z. Janout, *Phys. Lett.* **31B**, 405 (1970); **36B**, 501 (1971).

<sup>9</sup>N. E. Booth, G. Conforto, R. J. Esterling, J. Parry, J. Scheid, D. Sherden, and A. Yokosawa, *Phys. Rev. Lett.* **23**, 192 (1969).

<sup>10</sup>D. J. Sherden, N. E. Booth, G. Conforto, R. J. Esterling, J. Parry, J. Scheid, and A. Yokosawa, *Phys. Rev. Lett.* **25**, 898 (1970).

<sup>11</sup>J. Scheid, N. E. Booth, G. Conforto, R. J. Esterling, J. Parry, D. Sherden, and A. Yokosawa, *Phys. Rev. D* (to be published). Some results also appeared in *High Energy Collisions*, edited by C. N. Yang *et al.* (Gordon and Breach, New York, 1969), p. 51, and preliminary results appeared in *Phys. Rev. Lett.* **21**, 1410 (1968).

<sup>12</sup>N. E. Booth, G. Conforto, R. J. Esterling, J. Parry, J. Scheid, D. Sherden, and A. Yokosawa, *Phys. Rev. Lett.* **21**, 651 (1968). The small difference between the preliminary results and the final values presented here is due to renormalization of the target polarization and to other corrections mentioned in the text.

<sup>13</sup>The principles of operation of the polarized target are explained by A. Abragam [*The Principles of Nuclear Magnetism* (Clarendon Press, Oxford, England, 1961)] and C. D. Jeffries [*Dynamic Nuclear Orientation* (Interscience, New York, 1963)]. Specific design parameters of the target facility used in this experiment are given in the ZGS User's Manual.

<sup>14</sup>A. Moretti, S. Suwa, and A. Yokosawa, in the *Second International Symposium on Polarization Phenomena of Nucleons, Karlsruhe, 1965 Proceedings*, edited by P. Huber and H. Schopper (Birkhauser, Stuttgart, Germany, 1966), p. 128; F. Betz, J. Arens, O. Chamberlain, H. Dost, P. Grannis, M. Hansroul, L. Holloway, C. Schultz, and G. Shapiro, *Phys. Rev.* **148**, 1289 (1966).

<sup>15</sup>A. Beretvas, *Phys. Rev.* **171**, 1392 (1968); R. E. Hill, N. E. Booth, R. J. Esterling, S. Suwa and A. Yokosawa, *Phys. Rev. D* **1**, 729 (1970).

<sup>16</sup>Eugene William Beier, thesis, University of Illinois, 1966 (unpublished).

<sup>17</sup>For further details of the hodoscopes used, see C. L. Dolnick, *Nucl. Phys.* **B22**, 461 (1970).

<sup>18</sup>According to convention, the polarization in  $pp$  scattering is positive if, for target spin right, the outgoing

proton with the smaller deviation from the beam direction is preferentially scattered up.

<sup>19</sup>Y. Ducros, *Rev. Mod. Phys.* **39**, 531 (1967); see also Ref. 4.

<sup>20</sup>See for example D. M. Austin, W. H. Greiman, and W. Rarita, *Phys. Rev. D* **2**, 2613 (1970).

<sup>21</sup>L. C. Wang, *Phys. Rev.* **142**, 1187 (1966).

<sup>22</sup>Some constraints can be made, however, if the imaginary parts of the  $\phi_i$  are given by Pomeranchukon exchange. See K. H. Mütter, *Nucl. Phys.* **B27**, 73 (1971).

<sup>23</sup>For the exchange of a natural parity Regge trajectory  $\phi_1 = \phi_3$ , see C. Itzykson and M. Jacob, *Nuovo Cimento* **28**, 250 (1963).

<sup>24</sup>See, for example, the review articles of C. B. Chiu [*Rev. Mod. Phys.* **41**, 640 (1969)] and J. D. Jackson [*ibid.* **42**, 12 (1970)].

<sup>25</sup>T. T. Wu and C. N. Yang, *Phys. Rev.* **137**, B708 (1965); L. Durand III and R. Lipes, *Phys. Rev. Lett.* **20**, 637 (1968); T. T. Chou and C. N. Yang, *ibid.* **20**, 1213 (1968).

<sup>26</sup>C. B. Chiu and J. Finkelstein, *Nuovo Cimento* **57A**, 649 (1968); **59A**, 92 (1969); K. Huang and S. Pinsky, *Phys. Rev.* **174**, 1915 (1968); M. L. Blackmon and G. R.

Goldstein, *Phys. Rev. D* **1**, 2675 (1970).

<sup>27</sup>A. Capella, J. Kaplan, A. Krzywicki, and D. Schiff, *Nuovo Cimento* **63A**, 141 (1969).

<sup>28</sup>A. de-Shalit, in *Preludes in Theoretical Physics*, edited by A. de-Shalit, L. Van Hove, and H. Feshbach (North-Holland, Amsterdam, 1966), p. 35.

<sup>29</sup>M. Jacob and J. Weyers, *Nuovo Cimento* **66A**, 401 (1970).

<sup>30</sup>A. D. Krisch, *Phys. Rev. Lett.* **19**, 1149 (1967).

<sup>31</sup>J. H. Parry, thesis, University of Chicago (unpublished).

<sup>32</sup>S. Pinsky, *Phys. Rev. Lett.* **21**, 1776 (1968); E. J. Sacharidis, Rutherford High Energy Laboratory Report No. 186, 1969 (unpublished); G. C. Fox, in *High Energy Collisions*, edited by C. N. Yang *et al.* (Gordon and Breach, New York, 1969) p. 367.

<sup>33</sup>G. Alexander, O. Benary, and L. R. Price, LBL Report No. UCRL-20000 NN, 1970 (unpublished); A. N. Diddens, CERN report, Geneva, 1971 (to appear in Landolt-Börnstein).

<sup>34</sup>R. Odorico, A. Garcia, and C. A. Garcia-Canal, *Phys. Lett.* **32B**, 375 (1970).

## Elastic Electron-Proton Scattering at Large Four-Momentum Transfer\*

P. N. Kirk,<sup>†</sup> M. Breidenbach,<sup>‡</sup> J. I. Friedman, G. C. Hartmann,<sup>§</sup> and H. W. Kendall

*Department of Physics and Laboratory for Nuclear Science, Massachusetts Institute of Technology, Cambridge, Massachusetts 02139*

G. Buschhorn,<sup>||</sup> D. H. Coward, H. DeStaebler, R. A. Early, J. Litt,<sup>\*\*</sup> A. Minten,<sup>\*\*</sup> L. W. Mo,<sup>††</sup>  
W. K. H. Panofsky, and R. E. Taylor

*Stanford Linear Accelerator Center, Stanford, California 94305*

B. C. Barish, S. C. Loken,<sup>‡‡</sup> J. Mar,<sup>§§</sup> and J. Pine  
*California Institute of Technology, Pasadena, California 91109*

(Received 13 January 1972)

Electron-proton elastic-scattering cross sections have been measured at the Stanford Linear Accelerator Center for four-momentum transfers squared  $q^2$  from 1.0 to 25.0 (GeV/c)<sup>2</sup>. The electric ( $G_{Ep}$ ) and magnetic ( $G_{Mp}$ ) form factors of the proton were not separated, since angular distributions were not measured at each  $q^2$ . However, values for  $G_{Mp}$  were derived assuming various relations between  $G_{Ep}$  and  $G_{Mp}$ . Several theoretical models for the behavior of the proton magnetic form factor at high values of  $q^2$  are compared with the data.

### I. INTRODUCTION

Understanding the internal structures of elementary particles is a fundamental problem of strong-interaction physics. More than 15 years have elapsed since the early experiments of Hofstadter and collaborators at Stanford<sup>1</sup> showed the effects of the structure of the proton in elastic electron-proton scattering. During this time the problem of hadronic structure in general and nuclear structure in particular has received the attention of experimentalists and theorists alike. The proton is the easiest hadron to study, and

many available techniques can shed light on its structure. Of these techniques, high-energy elastic electron-proton scattering has proved to be particularly fruitful since the quantum electrodynamic portion of the interaction is understood.

The momentum carried by the virtual photon responsible for the elastic scattering is reciprocally related to its wavelength, and thus approximately reciprocally related to the characteristic distance probed in the interaction. One of the principal objectives of our experimental program was to make use of the high-energy and high-intensity electron beam at the Stanford Linear Ac-